

# Precision-engineered niche for directed differentiation of MSCs to lineage-restricted mineralized tissues

Journal of Tissue Engineering  
Volume 13: 1–14  
© The Author(s) 2022  
Article reuse guidelines:  
sagepub.com/journals-permissions  
DOI: 10.1177/20417314211073934  
journals.sagepub.com/home/tej



Saeed Ur Rahman<sup>1,2</sup>, Sasikumar Ponnusamy<sup>1</sup>,  
Malvika Nagrath<sup>1</sup> and Praveen R Arany<sup>1</sup> 

## Abstract

The major difference between tissue healing and regeneration is the extent of instructional cues available to precisely direct the biological response. A classic example is reparative or osteodentin that is seen in response to physicochemical injury to the pulp-dentin complex. Dentin regeneration can direct the differentiation of dental stem cells using concerted actions of both soluble (biomolecules, agonists, and antagonists) and insoluble (matrix topology) cues. The major purpose of this study was to examine the synergistic combination of two discrete biomaterial approaches by utilizing nanofiber scaffolds in discrete configurations (aligned or random) with incorporated polymeric microspheres capable of controlled release of growth factors. Further, to ensure appropriate disinfection for clinical use, Radio-Frequency Glow Discharge (RFGD) treatments were utilized, followed by seeding with a mesenchymal stem cell (MSC) line. SEM analysis revealed electrospinning generated controlled architectural features that significantly improved MSC adhesion and proliferation on the aligned nanofiber scaffolds compared to randomly oriented scaffolds. These responses were further enhanced by RFGD pre-treatments. These enhanced cell adhesion and proliferative responses could be attributed to matrix-induced Wnt signaling that was abrogated by pre-treatments with anti-Wnt3a neutralizing antibodies. Next, we incorporated controlled-release microspheres within these electrospun scaffolds with either TGF- $\beta$ 1 or BMP4. We observed that these scaffolds could selectively induce dentinogenic or osteogenic markers (DSPP, Runx2, and BSP) and mineralization. This work demonstrates the utility of a novel, modular combinatorial scaffold system capable of lineage-restricted differentiation into bone or dentin. Future validation of this scaffold system *in vivo* as a pulp capping agent represents an innovative dentin regenerative approach capable of preserving tooth pulp vitality.

## Keywords

Stem cells, electrospinning, nanofiber scaffolds, dentin, bone, TGF- $\beta$ 1, BMP-4

Date received: 22 October 2021; accepted: 31 December 2021

## Introduction

Dental biomaterials have been a mainstay of clinical dentistry. Progress in clinical techniques, instruments, and materials has pushed the boundaries from simply restoring oral-dental tissues to tissue regeneration. The pulp-dentin complex has been a central focus on harnessing bioengineering advances arising from material science, developmental, stem cells, and regenerative medicine.<sup>1</sup> The pulp-dentin complex responds to injury with the formation of a protective barrier termed osteodentin that has been a clinically acceptable outcome to effectively maintain tooth vitality. However, progress in dental stem cells and fundamental insights into odontogenic development

and regulation are enabling exciting approaches in promoting tissue healing to regenerative clinical applications.<sup>2,3</sup> Advances in material sciences have attempted to

<sup>1</sup>Oral Biology, Surgery and Biomedical Engineering, University at Buffalo, Buffalo, NY, USA

<sup>2</sup>Oral Biology, Institute of Basic Medical Sciences, Khyber Medical University, Peshawar, Pakistan

### Corresponding author:

Praveen R Arany, Oral Biology, Surgery and Biomedical Engineering, University at Buffalo, B36A Foster Hall, 3435 Main Street, Buffalo NY 14214, USA.

Email: prarany@buffalo.edu



generate an in situ niche that mimics natural biological architecture and functions.<sup>4</sup> These include cell functionalization, controlled delivery of growth factors, morphopatterning material interfaces, modular assembly, and microfluidics for vascular supply within these biomaterial scaffolds.<sup>5,6</sup>

The extracellular matrix (ECM) plays a critical role in directing cellular behavior and functions.<sup>7</sup> A major role of the ECM is to create a favorable physical microenvironment for cell adhesion, proliferation, and differentiation.<sup>8,9</sup> Moreover, all cells, with the notable exception of the hematopoietic lineage, require the continuous flow of signals from their physical adhesion to ECM for survival.<sup>10</sup> These exogenous signals are relayed via receptor-mediated signaling that epigenetically regulates cell functions. Another critical function of the ECM is to sequester and present various biomolecules in a sustained manner to modulate cell phenotypes.<sup>11</sup> These include growth or differentiation factors, regulatory nucleic acids, glycoproteins, and lipids, among others. Thus, the natural ECM plays two discrete but overlapping functions. These insoluble cues can be generated by various biomaterial techniques such as electrospinning, lithography, and 3D printing capable of generating topological features ranging from the nanoscale to centimeters. Among them, electrospinning involves the generation of polymer fibers that can generate nanoscale (~10 nm) fibers that mimic natural ECM. These nanotopological features are known to promote specific morphogen pathways evoking directed biological responses, including regeneration of skin, nerve, blood vessels, cartilage, bone, and dentin both in vitro and in vivo.<sup>12,13</sup>

Growth factors are potent biological ligands capable of inducing signaling pathways determining proliferation, differentiation, and migration.<sup>14</sup> Their widespread use in clinical tissue regeneration has been extensively documented. However, a major limitation to their current clinical use has been rapid degradation and indiscriminate kinetics leading to non-therapeutic and off-target effects. The use of polymeric encapsulation for controlled release systems provides a major avenue for spatiotemporal regulation, thereby improving safety and therapeutic efficacy. Several growth factors are known to play pivotal roles in odontogenic lineages commitment, differentiation, and maturation. These include fibroblast growth factor (FGFs), Wntless-related integration site (Wnts), sonic hedgehog (Shh), bone morphogenetic proteins (BMPs), and transforming growth factors- $\beta$  (TGF- $\beta$ ) that contribute to the development of a tooth in a precisely regulated manner.<sup>15</sup> TGF- $\beta$ s are a superfamily of growth factors with over 32 members that play critical roles in odontoblast differentiation and maintenance of dentin in health and disease conditions.<sup>16</sup> Both TGF- $\beta$ 1 and BMPs have been noted to promote mineralized tissue repair. However, their precise

roles in dentin repair and regeneration remain to be fully elucidated.<sup>17–20</sup>

We recently demonstrated the utility of TGF- $\beta$  and BMPs incorporated-scaffolds systems to selectively induce the odontogenic, osteogenic, and chondrogenic differentiation.<sup>21–23</sup> The use of growth factors and their small-molecule antagonists has enabled the generation of well-defined morphogen fields that promoted the differentiation of lineage-restricted fates of MSC lines. Besides the polymeric controlled release systems and defined media conditions, the biomaterial scaffold systems were generated by gas-foaming that generated macroporous systems with adequate perfusion for the composite tissue constructs. This biomaterial system demonstrated the ability to generate discrete growth factor morphogen fields, but based on its nanoporous nature, it lacked the precise topological cues to direct cell responses at the biomaterial interface. To overcome this, we employed electrospinning to generate polymeric nanofiber matrices that promote dental pulp stem cells to differentiate and induce biomineralization.<sup>24</sup>

This work, for the first time, combines these two discrete approaches by providing both topological cues from electrospun nanofiber scaffolds and morphogens-incorporated microspheres. Another critical concern for biomaterial clinical use is effective disinfection to prevent infections. It also examines the efficacy of radiofrequency-glow discharge treatments as an in-office clinical disinfection approach. These novel scaffold systems were iteratively generated characterized to develop a modular, clinically translatable biomaterial system to promote directed differentiation of dental stem cells to regenerate dentin.

## Materials and methods

### Cell culture

Mesenchymal stem cells (D1) (ATCC, Manassas, VA) were procured and cultured under recommended conditions in Dulbecco's Modified Eagle Medium (DMEM), 10% fetal bovine serum (FBS), and 100 units/mL penicillin and streptomycin in a 37°C incubator with 5% CO<sub>2</sub>.

### Microspheres synthesis

A double emulsion technique was used to synthesize microspheres with poly ( $\epsilon$ -caprolactone) (PCL) and poly (lactico-glycolic acid) (PLGA, 85:15) (both Sigma-Aldrich, St. Louis, MO) as described previously.<sup>21</sup> Briefly, a 100- $\mu$ L quantity of payloads (Protoporphyrin-IX, Fluorescein-conjugated immunoglobulin, Albumin, TGF- $\beta$ 1, or BMP4) were pipetted into 1 mL of 5% PCL or PLGA in ethyl acetate (Sigma-Aldrich, St. Louis, MO) and immediately sonicated (QSonica, Newtown, CT) for 1 min. A second emulsion composed of 1% polyvinyl acetate (PVA) (Sigma-Aldrich, St. Louis, MO) and 7% ethyl acetate was then

added and vortexed for 15 s. This emulsion was then added to a 1% PVA solution with continuous stirring for 3 h at room temperature, filtered through a 0.2  $\mu\text{m}$  filter (ThermoFisher Scientific, Waltham, MA), collected by centrifugation, freeze-dried (Labconco, Kansas City, MO), and stored at  $-20^{\circ}\text{C}$  till further use.

### *Fabrication of nanofibers scaffolds*

Poly ( $\epsilon$ -caprolactone) (PCL) or poly (lactic-co-glycolic acid) (PLGA) nanofibers were synthesized as described previously.<sup>13</sup> A homogeneous polymer solution (12% w/v) was prepared by dissolving the polymer in N, N-Dimethylformamide (DMF), and Chloroform (both from Sigma-Aldrich, St. Louis, MO) overnight at room temperature. Microspheres were incorporated within nanofiber scaffolds by combining 10% w/w solutions with complementary polymers, namely PCL microspheres in PLGA solution of PLGA microspheres in PCL solutions. For electrospinning, solutions in a 10 mL syringe with a 20 Gauge metallic needle were used at a high voltage of 30 kV. The flow rate of the polymer solution was 500  $\mu\text{L}/\text{h}$ , and the distance between the collector and needle tip was 20 cm. The drum rotational speeds were adjusted to 300 or 700 rpm for aligned and random nanofibers, respectively. Alignment of nanofibers at low speed could be attributed to the elimination of the whipping phase, as noted in prior studies.<sup>25–28</sup>

### *Scanning electron microscopy, focused ion beam, and emission desorption spectroscopy*

Scanning electron microscopy (SEM) analysis was performed to determine the morphology of the nanofibers and microspheres. Briefly, the nanofibers or microspheres were attached to the adhesive tape surface for strong holding. The samples were sputter-coated with gold for 120 s and examined using SEM (Hitachi, S-4700, Japan) with a voltage of 15 kV. A 30 keV Ga focused ion beam (Carl Zeiss Auriga Crossbeam, USA) was used to ablate the polymeric microspheres embedded within electrospun nanofibers, and elemental analysis was performed with an energy-dispersive X-Ray spectrophotometer (Oxford Instruments NanoAnalysis, USA).

### *Microsphere and nanofiber scaffold release studies*

To determine release kinetics, specific amounts (200 mg) of microspheres were added in 1.5 mL of Phosphate buffer saline (PBS), and the samples were incubated at  $37^{\circ}\text{C}$ . The supernatant (100  $\mu\text{L}$ ) was taken from each of the tubes at 1, 5, 7, 14, and 21 days and assessed using Bradford assay (Albumin) or fluorescence spectroscopy (PPIX or Fluorescein) for mean cumulative release or fluorescence imaging (ChemiDoc MP, Bio-Rad, Hercules, CA).

### *Radiofrequency glow discharge treatments (RFGDT)*

A partial air-vacuum RFGD device (PDC-32G, Harrick Scientific, USA) was used as per the manufacturer's instructions. The scaffolds were placed within the chamber and treated for 3 min and used to seed cells for further analyses.

### *Cell adhesion assay*

The cells were cultured on different substrates (solid or nanofibers) with a density of  $5 \times 10^4$  cells per well. After 5 h following cell seeding, 10  $\mu\text{L}$  of the sample were taken from each well to assess unattached versus attached cells.

### *Cell proliferation assay*

The electrospun nanofiber matrices were placed in a 24-well cell culture plate. A plastic ring was used to prevent the lifting of the nanofibers. The samples were sterilized under UV or radiofrequency glow discharge (RFGD) treatments. D1 Cells were seeded on samples at a density of  $2 \times 10^4$  cells/well. After 24 h, cells were incubated with AlamarBlue (10% v/v, ThermoFisherScientific, Waltham, MA), and fluorescence (560/590 nm) was assessed using a microplate reader (Spectramax, Molecular Devices, San Jose, CA) where cell numbers are represented as relative fluorescence units (RFUs).

### *RNA extraction*

Cells were seeded ( $5 \times 10^5$  cells per well of six well plates) on different substrates in triplicates. After 4 days, samples were washed with PBS, and TRIzol reagent (700  $\mu\text{L}/\text{well}$  Invitrogen) was added and mixed gently to lyse cells. The lysate was transferred to a microfuge tube, and Chloroform (700  $\mu\text{L}$ , Sigma) was added and vigorously vortexed for 15 s. Following incubation for 20 min on ice, samples were centrifuged at 14,000 rpm for 10 min at  $4^{\circ}\text{C}$ . The clear supernatant was transferred to a fresh tube, and 700  $\mu\text{L}$  Isopropanol (Sigma) was added to each sample and mixed gently. Then, the samples were centrifuged at 14,000 rpm for 10 min. The supernatant was discarded, and 700  $\mu\text{L}$  of 70% ethanol was added and again centrifuged for 5 min. The pellet was left to air-dry and resuspended each sample in 50  $\mu\text{L}$  double distilled water. The concentration of the extracted total RNA was measured using the NanoDrop (NanoDrop Technologies Inc., USA).

### *cDNA synthesis and quantitative real-time PCR*

The cells were seeded ( $5 \times 10^5$  cells per well of six well plates) on different substrates in triplicates for 4 days. Total RNAs were extracted using Trizole reagents, and cDNA was synthesized using a reverse transcriptase reagents kit

(Bio-Rad, Hercules, USA). Quantitative real-time PCR was performed on a Real-time PCR system (Applied Biosystems, Foster City, CA). Glyceraldehyde-3-phosphate dehydrogenase (GAPDH) gene expression was used as a control for normalizing the gene expression data.

### *Alizarin red staining*

Mineralization by D1 cells on different substrates was assessed with Alizarin Red S staining (Sigma-Aldrich, St. Louis, MO). Briefly, cells ( $1 \times 10^5$  cells per well) were seeded on six wells cell culture plates with or without nanofiber scaffolds. Following 2 weeks of culture, the samples were washed using cold PBS, fixed with 70% cold ethanol, washed again with deionized water, and stained with 40 mM Alizarin red S (pH 4.2) for 20 min at room temperature. Samples were rinsed, and digital images were captured on a transilluminator.

### *Statistical analysis*

The sample size was calculated, keeping the power of the study equal to 95% and the level of significance equal to 5%. Each group had been performed in replicates ( $n=3$ ), and all the experiments were repeated at least twice to confirm the accuracy and reproducibility. The data was organized in Excel (Microsoft, Redmond WA) and analyzed in Prism (GraphPad Prism, San Diego CA). Due to the limited sample size, non-parametric tests for independent groups Mann Whitney  $U$  test and multiple groups comparison Kruskal-Wallis test were used. Data is presented in the figures as mean  $\pm$  SD values where  $p < 0.05$  with Mann Whitney  $U$  test was considered significant.

## **Results**

### *Nanofibrous scaffolds generated by electrospinning with varying alignments*

Nanofibrous scaffolds mimic the natural ECM, which provides a physical and biological microenvironment for guiding cell proliferation and differentiation. The physical microenvironment plays an essential role in odontoblast functions during development and repair. It has been suggested that ECM's nanotopography or orientation features are able to regulate the morphology and function of stem cells via specific cell-surface interactions.<sup>29</sup> Aligned matrices offer improved mechanical properties such as higher tensile modulus and ultimate tensile strength than that the random nanofiber. Furthermore, it has also been documented that cell spreading and collagen expression are significantly higher in the aligned regions than randomly aligned nanofibers.<sup>30,31</sup> We first generated nanofiber scaffolds with both PLGA and PCL in random and aligned fibers by electrospinning. SEM analyses confirmed both

aligned and randomly oriented nanofiber scaffolds could be selectively generated (Figure 1(a)). Population distributions analyses of both patterns of scaffolds noted variations in fibers diameter and highly uniform nanofibers that were more aligned with PCL and less with PLGA (Figure 1(b)). The average diameter of PCLF-random was 583 nm, PCLF-aligned 787 nm, PLGAF-random 1140 nm, and PLGAF-aligned was 1110 nm.

### *Nanofibrous scaffolds enhanced Wnt signaling-induced cell proliferation*

Nanofiber orientation is known to affect cell adhesion, morphology, and cell proliferation. We examined these responses in an MSC cell line, D1, on these scaffolds.<sup>32</sup> We observed a significant increase in cell adhesion on both patterns of nanofiber scaffolds compared to solid substrates ( $n=3$ ,  $p < 0.05$ ) (Figure 2(a)). Aligned nanofiber demonstrated better (92%) cells adhesion compared to random (84%) nanofibers ( $p < 0.05$ ). Further, cell proliferation on these scaffolds also demonstrated a similar increase in both nanofiber patterns compared to a solid substrate ( $n=3$ ,  $p < 0.05$ ) (Figure 2(b)). To investigate these proliferative responses, we next sought to examine specific signaling pathways that may be involved at the material interface. Previously, we have demonstrated that nanofibrous scaffolds induce canonical Wnt signaling pathways in mesenchymal stem cells.<sup>24</sup> Transgenic activation of Wnt signaling in the epithelium during development has been noted to induce supernumerary placodes and extra teeth.<sup>33</sup> Supporting these pro-survival roles, Wnt3a increased secretory odontoblasts in a pulp injury model.<sup>34</sup> Therefore, we first examined the effects of Wnt signaling on D1 cells. We noted Wnt3a was capable of inducing a significant proliferative response in these cells ( $p < 0.05$ ) (Figure 2(c)). Next, we inquired if the proliferative response in nanofiber scaffolds could be mediated via Wnt signaling by preincubating cells with anti-Wnt3a antibodies prior to seeding. We observed a complete abrogation of the proliferative responses (Figure 2(d)). These results indicate that the nanofiber topology is capable of inducing Wnt signaling that can expand stem cell populations to aid in tissue regeneration.

### *RFGD treatment enhanced nanofiber-induced cells function*

Nanofiber scaffolds mimicking the natural ECM have garnered much interest in bioengineering and wound healing. However, there have been concerns regarding their biocompatibility and practical clinical use. Several post-fabrication approaches have been utilized to improve these mechanical properties.<sup>35</sup> Radiofrequency glow discharge treatment (RFGDT) has been used to disinfect and improve the hydrophilicity of biomaterials. Pre-treatments of

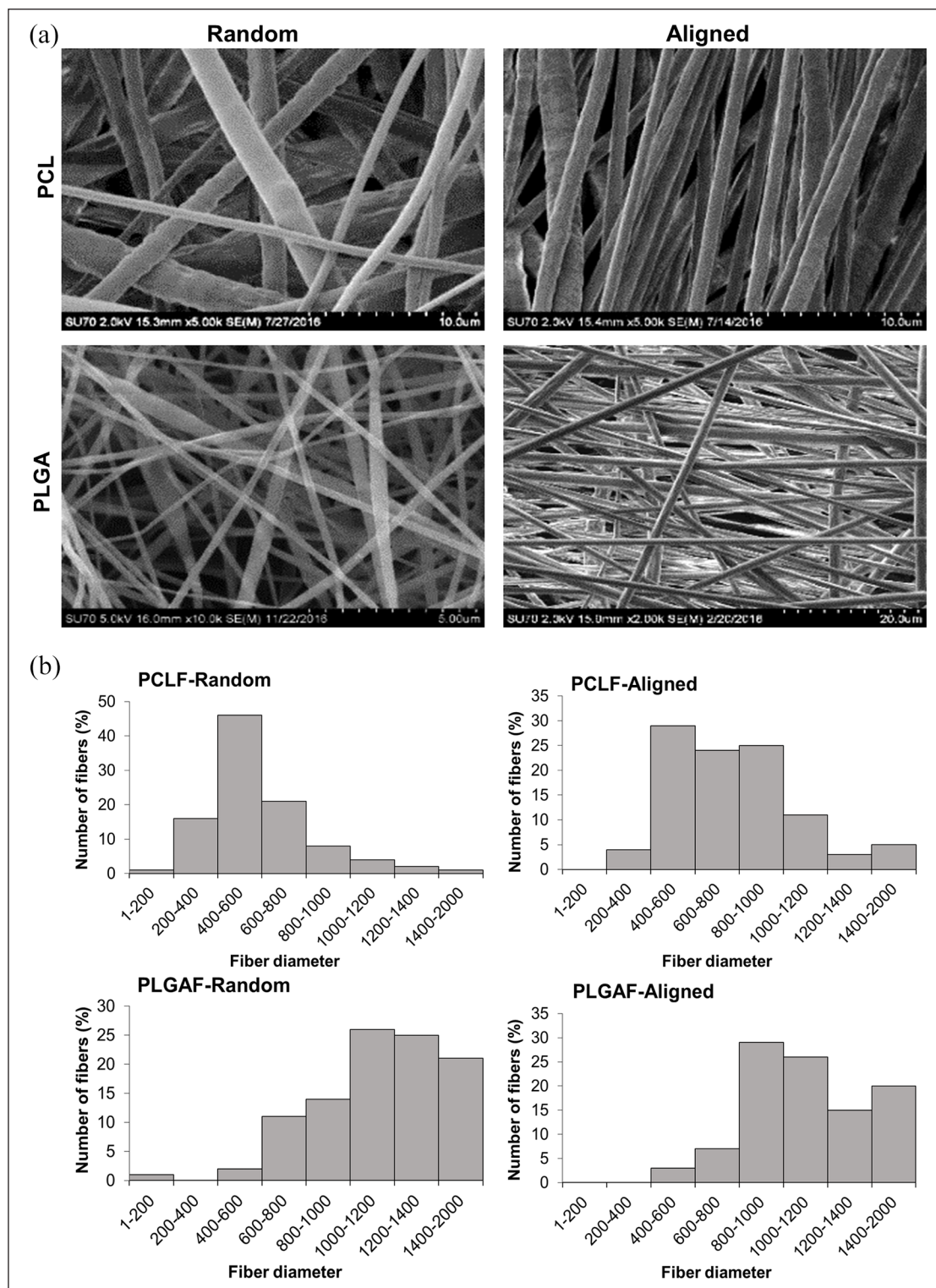


**Figure 1.** Electrospun nanofiber scaffolds with varying topology: (a) SEM micrographs show random and aligned oriented nanofibers of Poly  $\epsilon$ -caprolactone (PCLF) and Poly(lactic co-glycolic acid) (PLGAF) and (b) SEM images were digitally quantified for fiber diameter and size distribution.

biomaterials with RFGDT have been noted to increase osteoblast cell functions and gene expression.<sup>36</sup> Hence, we examined the effects of RFGDT on our electrospun nanofiber scaffolds. We observed that the improved cell

adhesion in both nanofiber patterns was further significantly enhanced following RFGDT ( $n=3$ ,  $p<0.05$ ) (Figure 3(a)). We then examined cell proliferation and noted a similar significant increase in cell numbers on both

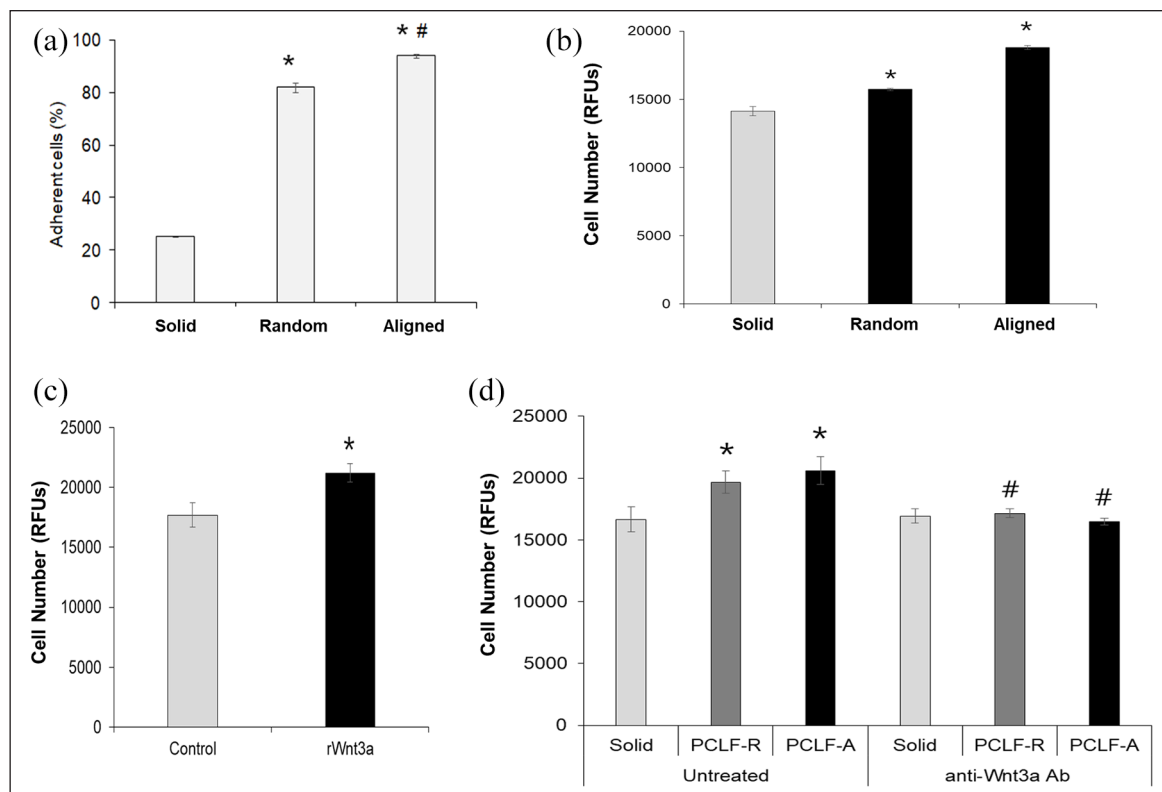


**Figure 2.** Nanotopology substrates induce cell adhesion and proliferation: (a) D1 cell adhesion on different substrates such as solid surface, PCLF-random, and PCLF-aligned nanofibers was assessed, (b) cells were cultured on solid, PCLF-R, and PCLF-A for 24 h and cell proliferation was determined using AlmarBlue assay, (c) cells were treated with recombinant Wnt3a protein (100 ng/mL) for 24 h and cell proliferation was determined, and (d) incubation with anti-Wnt3a neutralizing antibodies was performed to examine effects of Wnt signaling on cell proliferation from various polymeric substrates. Data are presented as Mean  $\pm$  SD where  $n=3$ , and  $p < 0.05$  was considered statistically significant from control (\*) and untreated group (#).

nanopatterned scaffolds following RFGDT compared to a solid substrate ( $n=3$ ,  $p < 0.05$ ) (Figure 3(b)). It is prudent to emphasize that the aligned nanopatterned scaffolds performed even better than the random scaffold following RFGDT. Prior studies have noted that MSCs on RFGD treated nanofibers demonstrate improved viability and differentiation.<sup>37</sup> As our scaffolds demonstrated a similar response, we examined mineralized tissue differentiation in D1 with routine induction media. These nanofiber scaffolds induced robust mineralization compared to solid substrates that were more prominent following RFGDT (Figure 3(c)). Among them, the aligned RFGDT scaffolds performed best overall, even after normalizing to the observed increase in cell numbers (Figure 3(d)). Overall, these studies demonstrated the utility of RFGDT on aligned nanofiber scaffolds to optimally induce stem cell adhesion, proliferation, and differentiation.

### Nanofibers are capable of inducing odontoblast or osteoblast differentiation

One of the important components of tissue engineering is the cell source. The origin of dental stem cells has been

attributed to the neural crest and the perivascular niche but remains to be fully elucidated.<sup>38</sup> These cells have been clearly demonstrated to be capable of multi-lineage differentiation and, most relevantly, into several relevant craniofacial mineralized tissues such as bone, cementum, and dentin. We had previously noted the D1 cells are capable of being directed to odontogenic and osteogenic fates.<sup>21,22</sup> Hence, we utilized RFGD-treated aligned PCL and PLGA scaffolds seeded with D1 cells and performed real-time qPCR analyses for DSPP, BSP, and Runx2 expression after 4 days. We observed significant induction of dentin matrix marker, DSPP in both scaffolds compared to non-RFGD treated aligned scaffolds and solid substrates ( $n=3$ ,  $p < 0.05$ ) (Figure 4(a) and (b)). Similarly, a key mineralized tissue transcription factor, Runx2, was induced by both PCL and PLGA aligned nanofiber scaffolds that had been RFGD-treated (Figure 4(c) and (d)). In contrast to these, the RFGD-treated PLGA nanofiber scaffolds showed a dramatically stronger induction of the bone transcription factor, BSP, compared to the PCL scaffolds (Figure 4(e) and (f)). These results suggest that biomaterial composition and nanotopology play an important role in determining lineage fate responses in mineralized tissue differentiation.

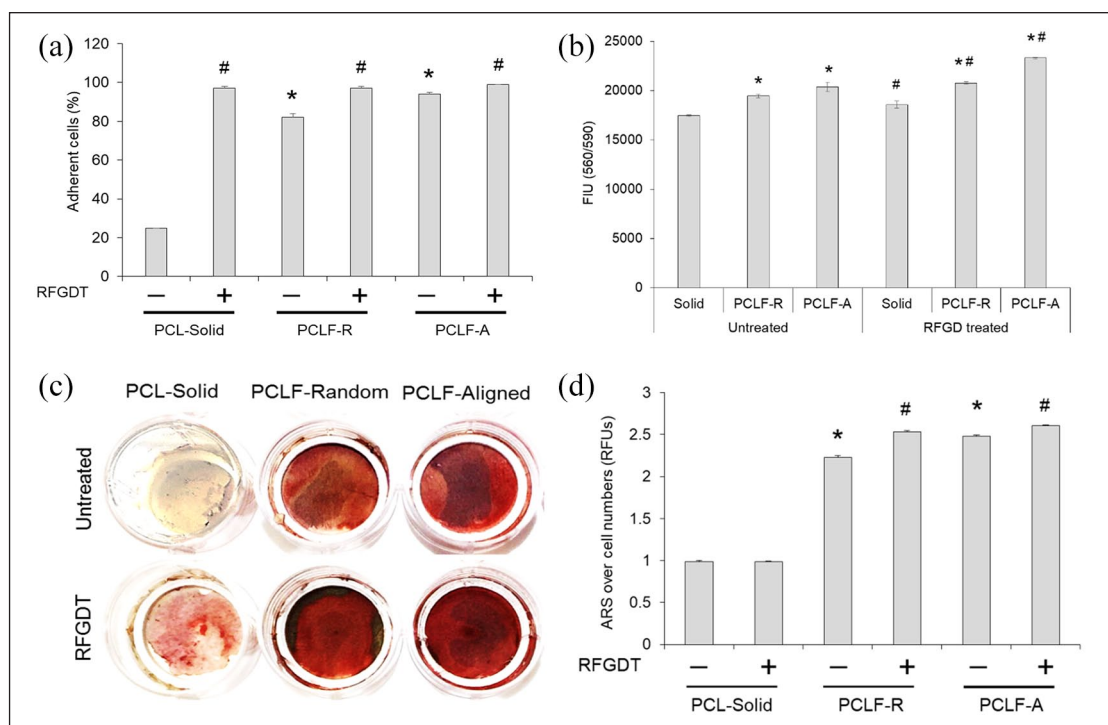


**Figure 3.** RFGDT improves nanofiber responses (a). Different PCL substrates such as solid, random (PCLF-R), and aligned (PCLF-A) nanofibers were treated with RFGD, and D1 cells were cultured. After 5 h post-seeding, the supernatant was assessed for non-adherent cells (b). Cells were cultured with or without RFGD-treatments, and cell proliferation was assessed after 24 h with AlamarBlue assay (c). Cells were seeded on these substrates for 14 days and examined for mineral deposition using Alizarin Red staining. (d) Digital images were quantified by densitometry, and data were normalized to cell numbers from the prior assay. Data are presented as Mean  $\pm$  SD,  $n=3$ , and  $p < 0.05$  was considered statistically significant from control (\*) and untreated group (#).

### A controlled delivery system for regenerative dentin cues

Growth factors are involved in many cellular functions and the differentiation of stem cells. Another key factor in dentin formation is TGF- $\beta$ s that have been shown to drive odontoblast differentiation, development, and repair.<sup>39</sup> Attempts at utilizing recombinant TGF- $\beta$  in various formulations have shown variable success in dental pulp capping studies.<sup>40</sup> Conditional loss of Smad4, the shared TGF- $\beta$ /BMP cytoplasmic signaling intermediate, from the dental papilla was noted to prevent terminal differentiation of odontoblasts and dentin deposition.<sup>41</sup> Further, overexpression of TGF- $\beta$ 1 generates dentin defects.<sup>42</sup> During dentin repair, a bone-like phenotype or osteodentin is evident. A major growth factor driving bone differentiation is Bone Morphogenetic Proteins (BMPs) that also contribute to early dentin development.<sup>3,19,43</sup> Thus, this evidence suggests that precise presentation of TGF- $\beta$ 1 and BMP are essential to harness their therapeutic roles for dentin regeneration.

We have recently demonstrated the utility of polymeric microspheres capable of generating controlled, sustained release of morphogens with both TGF- $\beta$  and BMPs.<sup>21,22</sup> In this study, we first generated PCL and PLGA microspheres and examined them with SEM (Figure 5(a) and (b)). Next, we incorporated these microspheres within the electrospun

nanofiber scaffolds and examined their ability to release prototypical biological payloads. Bovine Serum Albumin (BSA) is routinely used as a recombinant growth factor carrier.<sup>44-46</sup> It also represents a readily available, affordable prototypical protein payload (66.5 kDa) that can be easily assessed with Bradford assay for release studies. Hence, we chose to use BSA to demonstrate the effectiveness of the payload delivery from microspheres within electrospun nanofiber scaffolds. We observed a slow, sustained release from PLGA microspheres-PCL scaffolds (Figure 5(c)), while there was a delayed, burst release from PCL microspheres-PLGA scaffolds (Figure 5(d)). To further validate this system, we also incorporated a fluorescein-tagged immunoglobulin (110kDa) and observed similar release kinetics with both scaffold systems (Figure 5(e) and (f)). These release kinetics and our prior work enabled us to determine precise concentrations of the growth factors TGF- $\beta$ 1 (25 kDa) and BMP4 (34 kDa) to generate sustained signaling within our scaffold systems.<sup>21,22</sup>

### Validation of microspheres within electrospun scaffolds

The polymeric microspheres are incorporated into their respective matrix polymers solutions immediately prior to electrospinning, minimizing their exposure to the solvent.

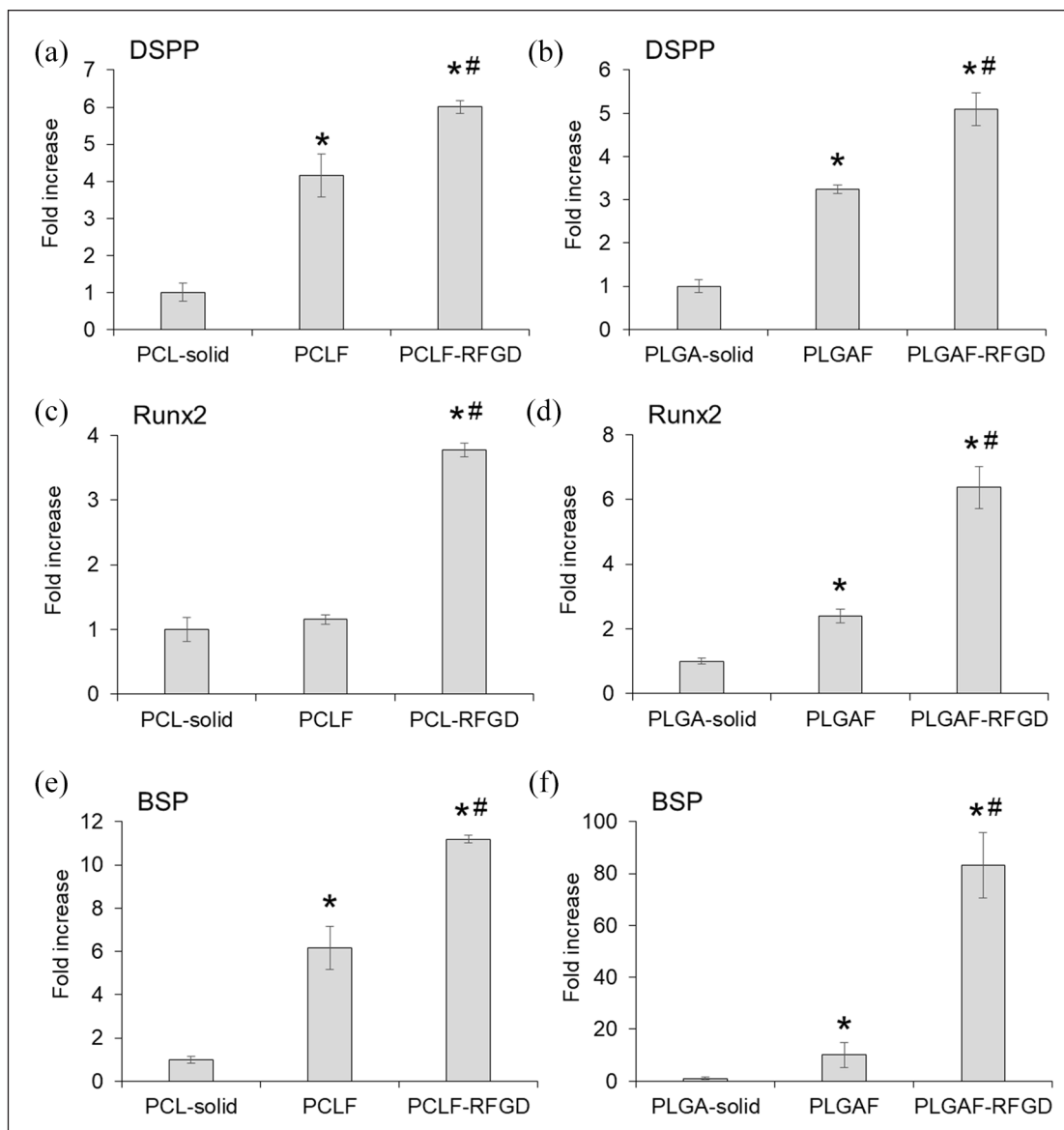


**Figure 4.** Nanofibers scaffolds induce osteoblast and odontoblast differentiation. DI cells were cultured on untreated or RFGD-treated aligned nanofiber substrates, and gene expressions were examined after 4 days of culture by quantitative real-time PCR analysis showing normalized expression over GAPDH of (a) DSPP on PCLF, (b) DSPP on PLGAF, (c) Runx2 on PCLF, (d) Runx2 on PLGAF, (e) BSP on PCLF, and (f) BSP on PLGAF. Data are presented as Mean  $\pm$  SD where  $n=3$ , and  $p < 0.05$  was considered statistically significant from control (\*) and untreated group (#).

To effectively visualize the incorporation of the microspheres, we first generated two fluorescent payloads, hematoporphyrin (PPIX) and fluorescein-conjugated immunoglobulin, and performed electrospinning. We observed discrete fluorescence signals in these scaffolds that demonstrated the uniform, largely homogenous distribution of the polymeric microspheres within the electrospun scaffolds (Figure 6(a) and (b)). SEM demonstrated the successful incorporation of microspheres into these electrospun nanofibers as local dilatations (Figure 6(c) and (e)). To further characterize these scaffolds, the dilatations were identified by SEM were dissected with a focused ion

beam, and emission desorption spectroscopy (EDS) was performed. We noted a subtle change in the polymeric composition between the PLGA ( $C_3H_8O_5$ ) versus PCL ( $C_6H_{10}O_2$ ) (Figure 6(d) and (f)). As the EDS mapping was not very discrete with these scaffolds, we utilized sodium chloride-encapsulated PLGA microspheres and noted a subtle increase in sodium levels in the microsphere walls embedded within the polymeric fiber (Supplemental Figure 1). These results confirmed that these electrospun nanofiber systems had microspheres incorporated capable of releasing growth factors and generating morphogen fields consistently within them.

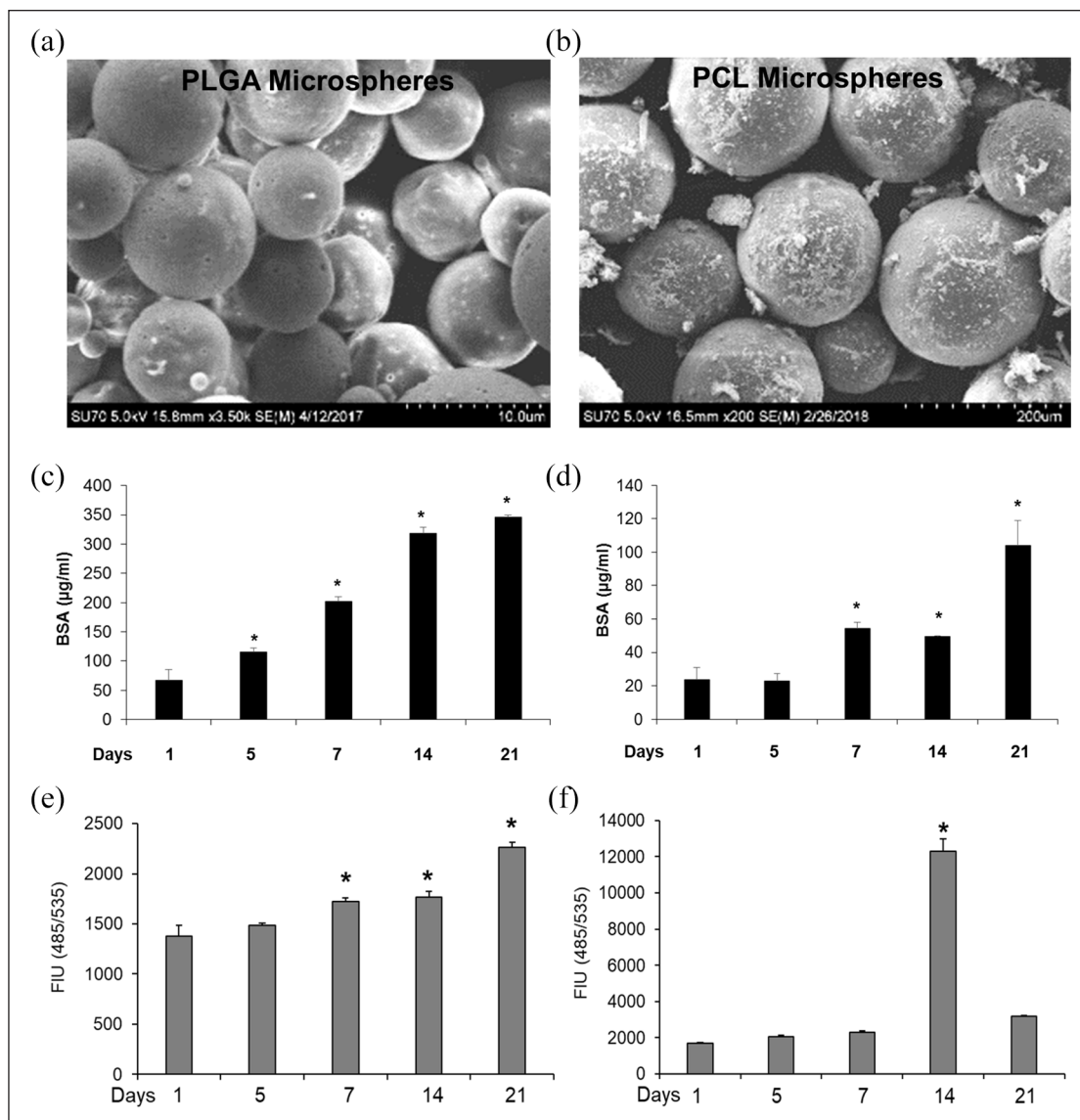


**Figure 5.** Controlled-release polymeric microspheres incorporated into nanofiber scaffolds: (a) SEM image of PLGA microspheres, (b) SEM image PCL microspheres, (c) release kinetics for bovine serum albumin from PLGA microspheres incorporated in PCL nanofiber scaffolds, (d) release kinetics for bovine serum albumin from PCL microspheres incorporated in PLGA nanofiber scaffolds, (e) release kinetics for fluorescein-conjugated immunoglobulin from PLGA microspheres incorporated in PCL nanofiber scaffolds, and (f) release kinetics for fluorescein-conjugated immunoglobulin from PCL microspheres incorporated in PLGA nanofiber scaffolds. Data are presented as Mean  $\pm$  SD where  $n = 3$ , and  $p < 0.05$  was considered statistically significant from day 1 (\*).

### Morphogens-incorporated nanofibers induce osteodentin differentiation

Based on these results, we finally chose to proceed with the RFGD-treated aligned nanofiber PCL scaffolds to evaluate both TGF- $\beta$ 1 and BMP containing PLGA microspheres for dentin induction. Gene expression using quantitatively real-time PCR analysis noted that D1 cells grown with TGF- $\beta$ 1 nanofiber scaffolds had a prominent dentin phenotype with elevated levels of DSPP and Runx2 with reduced levels of BSP ( $n = 3$ ,  $p < 0.05$ ) (Figure 7(a)–(c)). In contrast, BMP-4 nanofiber scaffolds demonstrated a

more osteogenic phenotype with lower DSPP but higher Runx2 and BSP expression. It is worth highlighting that both Runx2 and BSP also have a role, *albeit* minor, in a dentin matrix organization. Overall, these morphogen-incorporated nanofiber systems demonstrated promising utility in directing dentin differentiation of stem cells.

### Discussion

Tooth decay and gum disease are amongst the most prevalent human disease. Despite being completely preventable by good oral hygiene and proper diet, a lack of access to



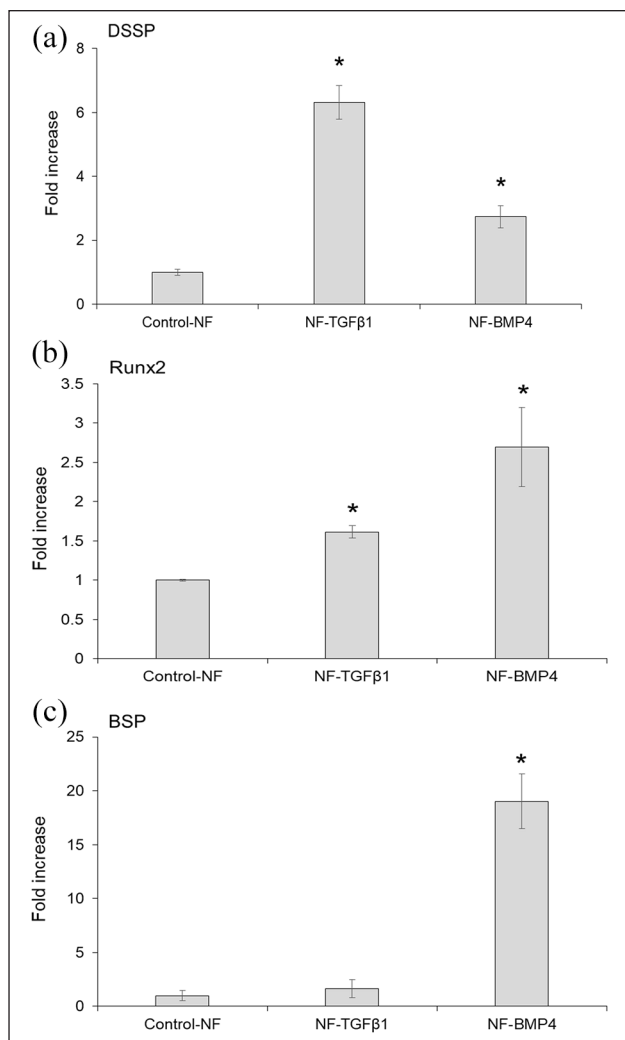


**Figure 7.** Directed gene expression in stem cells on composite nanofiber scaffolds. D1 cells were seeded on D1 cells were cultured on RFGD treated aligned PCL nanofiber scaffolds with PLGA microspheres with either TGF- $\beta$ 1 or BMP-4 for 4 days, and quantitative real-time PCR analysis was performed to examine normalized expression over GAPDH of (a) DSSP, (b) Runx2, and (c) BSP. Data are presented as Mean  $\pm$  SD where  $n=3$  and  $p < 0.05$  are considered statistically significant from control (\*).

the replacement of natural craniofacial tissues is unfortunately prone to eventual material failure over time. There is an emerging emphasis on regeneration, rather than restoration alone, that is leading a paradigm shift in clinical dentistry.<sup>51</sup> A major inspiration for these initiatives is based on biomimetic materials that naturally reproduce normal form and function. Broadly, these design features emphasize the precise configurations for the soluble (biomolecules) and insoluble (material topology) cues within these biomaterial systems for functional tissues and organ systems.<sup>52–54</sup> We recently demonstrated the ability of photoactivated latent TGF- $\beta$ 1 directs differentiation of dental stem cells to generate

osteodentin.<sup>23</sup> The significance of regenerative dentistry aims to retain the structure and strength of the tooth while preserving pulp vitality.

The controlled and sustained delivery of regenerative factors can be achieved via biomaterial scaffold systems. These biomaterial delivery systems and their degradation byproducts should be non-cytotoxic and biocompatible to prevent adverse local tissue responses that may delay tissue regeneration. Further, a significant component in designing a sustained and controlled delivery system is the selection of the appropriate molecule or their combinations for optimal tissue repair.<sup>55</sup> Thus, a suitable biomaterial system must satisfy several physical and biological constraints for use as a successful delivery system.<sup>56</sup> The current work was motivated by two major needs. First, to generate a specialized biomaterial interface that would promote stem cells in the pulp-dentin complex to expand that are lost due to caries or mechanical excavation. We generated nanofiber scaffolds by electrospinning to recapitulate the natural ECM that enabled cell adhesion, increased cell numbers, and eventually fostered directed differentiation of dentin. In this study, we noted the material interfaces consisting of aligned nanofibers ranging from 10 to 1000 nm were capable of inducing Wnt signaling and expanding stem cells. This is a key step for successful pulp-dentin repair due to injuries or infections reducing mature odontoblasts in the region. The multifunctional scaffolds described in this study can serve as novel pulp-capping agents and add to current conventional approaches with calcium hydroxide or mineral trioxide aggregate. In keeping with our practical goals of clinical translation, a key concern with these custom-designed biomaterial scaffolds is the ability to disinfect them prior to clinical use effectively. RFGDT appears to serve as an effective non-destructive strategy to disinfect biomaterial scaffolds while concurrently improving MSC expansion. Additionally, the use of RFGDT enhanced the cell adhesion and long-term mineralization responses suggesting its additional benefits in improving the biomaterial niche.

A second motivation for this study was to develop a modular in vitro model system that would aid the investigation of the intermediate osteodentin phenotype. A precise understanding of this phenomenon would allow us to further examine plausible strategies from current repair to regeneration. The use of microsphere-encapsulated growth factors permitted the spatiotemporal presentation of two potent morphogens, TGF- $\beta$  and BMP, that are centrally involved in mineralized craniofacial tissue development and regeneration.<sup>57</sup> The current study noted that incorporation of the TGF- $\beta$ 1 and BMP4 microspheres minimally altered (small dilatations or beading  $\sim$ 300 nm) the morphology of the electrospun nanofibers. It is interesting to note that both material systems examined appear to be capable of expanding stem cells and promoting mineralized tissue phenotype, the material composition

(PLGA vs PCL). The viability of the growth factor payloads after electrospinning is evident by their ability to induce matrix-specific gene expression, as has been established by others as well.<sup>58–60</sup> The combination of the specific morphogen (BMP4 vs TGF- $\beta$ 1) appeared to promote a more osteogenic, perhaps osteodentin-like, rather than dentin phenotype that is currently being investigated. This may provide a future strategy where BMP actions could be blocked (e.g. small molecule inhibitors like Dorsomorphin) to promote a more regenerative dentin maturation phenotype with TGF- $\beta$ 1 signaling.

The results of this study outline the feasibility of sequentially directing individual, phased, pulp-dentin regenerative processes. This includes initial dental stem cell expansion, lineage-specific organic matrix secretion, and mineralized differentiation. While these are important dentin regenerative goals, a few limitations are evident. The ultimate dentin regenerative phenotype is to generate tubular dentin with neuroproprioception to retain tooth vitality. It is assumed that the nanopatterning will assist in tubular odontoblastic extension and polarization that remains to be demonstrated. Further, given the complexity of in vivo scenarios, both under sterile pulp exposure and with pre-existing infection (caries), mitigating the inflammatory and host immune responses remains to be specifically investigated. Finally, although both biomaterials (PLA and PLGA) used in this study have been extensively used in vivo previously, practical clinical implications for the novel pulp-capping system described here will need to address clinical biomechanical characteristics. This includes material degradation, mechanical strength, and wear when placed under intermediate or permanent restorations. However, an alternate exciting future avenue could be the incorporation of the fundamental findings such as topological (nanopatterning), spatiotemporal delivery (combination of soluble morphogens and their antagonists, immunomodulators, or antimicrobials), or both within conventional dental restorative materials. Studies examining these possibilities in well-designed, controlled animal studies are essential prior to practical use in human clinical scenarios.

## Conclusions

This study demonstrated that the use of a combinatorial approach with biomaterial nanopatterning and controlled-release morphogens to direct the differentiation of stem cells to an odonto- or osteoblast fate. Given the limited mechanical strength of these electrospun scaffolds, ongoing work is exploring 3D-printed restorative strategies to improve clinical performance in rodent models of pulp capping. The ability to preserve tooth vitality with these biomaterials-based pulp capping approaches appears to have significant potential for clinical dentistry as it represents a precise regenerative strategy compared to conventional restorative replacements.

## Declaration of conflicting interests

The author(s) declared no potential conflicts of interest with respect to the research, authorship, and/or publication of this article.

## Funding

The author(s) disclosed receipt of the following financial support for the research, authorship, and/or publication of this article: The authors wish to acknowledge the financial support (PRA) faculty startup funds from University at Buffalo. We thank Dr. Yueling Qin, BioDesign Core Facility, University at Buffalo, for help with SEM-FIB-EDS analysis.

## ORCID iD

Praveen R Arany  <https://orcid.org/0000-0002-6116-2340>

## Supplemental material

Supplemental material for this article is available online.

## References

1. Murray PE, Garcia-Godoy F and Hargreaves KM. Regenerative endodontics: a review of current status and a call for action. *J Endod* 2007; 33(4): 377–390.
2. Gronthos S, Brahim J, Li W, et al. Stem cell properties of human dental pulp stem cells. *J Dent Res* 2002; 81(8): 531–535.
3. Thesleff I and Sharpe P. Signalling networks regulating dental development. *Mech Dev* 1997; 67(2): 111–123.
4. Discher DE, Mooney DJ and Zandstra PW. Growth factors, matrices, and forces combine and control stem cells. *Science* 2009; 324(5935): 1673–1677.
5. Hendrickx B, Vranckx JJ and Lutun A. Cell-based vascularization strategies for skin tissue engineering. *Tissue Eng Part B Rev* 2011; 17(1): 13–24.
6. Lovett M, Lee K, Edwards A, et al. Vascularization strategies for tissue engineering. *Tissue Eng Part B Rev* 2009; 15(3): 353–370.
7. Langer R and Tirrell DA. Designing materials for biology and medicine. *Nature* 2004; 428(6982): 487–492.
8. Li WJ, Laurencin CT, Cateston EJ, et al. Electrospun nanofibrous structure: a novel scaffold for tissue engineering. *J Biomed Mater Res* 2002; 60(4): 613–621.
9. Ma PX. Scaffolds for tissue fabrication. *Mater Today* 2004; 7(5): 30–40.
10. Guilak F, Cohen DM, Estes BT, et al. Control of stem cell fate by physical interactions with the extracellular matrix. *Cell Stem Cell* 2009; 5(1): 17–26.
11. Taipale J and Keski-Oja J. Growth factors in the extracellular matrix. *FASEB J* 1997; 11(1): 51–59.
12. Barnes CP, Sell SA, Boland ED, et al. Nanofiber technology: designing the next generation of tissue engineering scaffolds. *Adv Drug Deliv Rev* 2007; 59(14): 1413–1433.
13. Yao Q, Cosme JG, Xu T, et al. Three dimensional electrospun PCL/PLA blend nanofibrous scaffolds with significantly improved stem cells osteogenic differentiation and cranial bone formation. *Biomaterials* 2017; 115: 115–127.
14. Wartlick O, Kicheva A and González-Gaitán M. Morphogen gradient formation. *Cold Spring Harb Perspect Biol* 2009; 1(3): a001255.

15. Wang Y, Li L, Zheng Y, et al. BMP activity is required for tooth development from the lamina to bud stage. *J Dent Res* 2012; 91(7): 690–695.
16. Smith AJ. Vitality of the dentin-pulp complex in health and disease: growth factors as key mediators. *J Dent Educ* 2003; 67(6): 678–689.
17. Dobie K, Smith G, Sloan AJ, et al. Effects of alginate hydrogels and TGF-beta 1 on human dental pulp repair in vitro. *Connect Tissue Res* 2002; 43(2–3): 387–390.
18. Nie X, Tian W, Zhang Y, et al. Induction of transforming growth factor-beta 1 on dentine pulp cells in different culture patterns. *Cell Biol Int* 2006; 30(4): 295–300.
19. Six N, Lasfargues JJ and Goldberg M. Differential repair responses in the coronal and radicular areas of the exposed rat molar pulp induced by recombinant human bone morphogenetic protein 7 (osteogenic protein 1). *Arch Oral Biol* 2002; 47(3): 177–187.
20. Wang W, Dang M, Zhang Z, et al. Dentin regeneration by stem cells of apical papilla on injectable nanofibrous microspheres and stimulated by controlled BMP-2 release. *Acta Biomater* 2016; 36: 63–72.
21. Arany PR, Huang GX, Gadish O, et al. Multi-lineage MSC differentiation via engineered morphogen fields. *J Dent Res* 2014; 93(12): 1250–1257.
22. Huang GX, Arany PR and Mooney DJ. Modeling and validation of multilayer poly(lactide-co-glycolide) scaffolds for in vitro directed differentiation of juxtaposed cartilage and bone. *Tissue Eng Part A* 2015; 21(15–16): 2228–2240.
23. Arany PR, Cho A, Hunt TD, et al. Photoactivation of endogenous latent transforming growth factor- $\beta$ 1 directs dental stem cell differentiation for regeneration. *Sci Transl Med* 2014; 6(238): 238ra69.
24. Rahman SU, Oh JH, Cho Y-D, et al. Fibrous topography-potentiated canonical Wnt signaling directs the odontoblastic differentiation of dental pulp-derived stem cells. *ACS Appl Mater Interfaces* 2018; 10(21): 17526–17541.
25. Kim JI, Hwang TI, Aguilar LE, et al. A controlled design of aligned and random nanofibers for 3D bi-functionalized nerve conduits fabricated via a novel electrospinning set-up. *Sci Rep* 2016; 6(1): 2376.
26. Leach MK, Feng ZQ, Tuck SJ, et al. Electrospinning fundamentals: optimizing solution and apparatus parameters. *J Vis Exp* 2011; 2011(47): e2494.
27. Kiselev P and Rosell-Llompart J. Highly aligned electrospun nanofibers by elimination of the whipping motion. *J Appl Polym Sci* 2012; 125(3): 2433–2441.
28. Yu H, Li Y, Song Y, et al. Ultralong well-aligned TiO<sub>2</sub>:Ln<sup>3+</sup> (Ln=Eu, Sm, or Er) fibres prepared by modified electrospinning and their temperature-dependent luminescence. *Sci Rep* 2017; 7: 44099.
29. Badyalak SF. The extracellular matrix as a scaffold for tissue reconstruction. *Semin Cell Dev Biol* 2002; 13(5): 377–383.
30. Gu BK, Park SJ and Kim CH. Beneficial effect of aligned nanofiber scaffolds with electrical conductivity for the directional guide of cells. *J Biomater Sci Polym Ed* 2018; 29(7–9): 1053–1065.
31. Lin Z, Zhao X, Chen S, et al. Osteogenic and tenogenic induction of hBMSCs by an integrated nanofibrous scaffold with chemical and structural mimicry of the bone-ligament connection. *J Mater Chem B* 2017; 5(5): 1015–1027.
32. Kuppan P, Sethuraman S and Krishnan UM. Interaction of human smooth muscle cells with nanofibrous scaffolds: effect of fiber orientation on cell adhesion, proliferation, and functional gene expression. *J Biomed Mater Res A* 2015; 103(7): 2236–2250.
33. Aoki K and Taketo MM. Tissue-specific transgenic, conditional knockout and knock-in mice of genes in the canonical Wnt signaling pathway. *Methods Mol Biol* 2008; 468: 307–331.
34. Hunter DJ, Bardet C, Mouraret S, et al. Wnt acts as a pro-survival signal to enhance dentin regeneration. *J Bone Miner Res* 2015; 30(7): 1150–1159.
35. Martelli G, Bloise N, Merletti A, et al. Combining biologically active  $\beta$ -lactams integrin agonists with poly(l-lactic acid) nanofibers: enhancement of human mesenchymal stem cell adhesion. *Biomacromolecules* 2020; 21(3): 1157–1170.
36. Rapuano BE, Hackshaw K and MacDonald DE. Heat or radiofrequency plasma glow discharge treatment of a titanium alloy stimulates osteoblast gene expression in the MC3T3 osteoprogenitor cell line. *J Periodontal Implant Sci* 2012; 42(3): 95.
37. Ardeshiryajimi A, Dinavand P, Seyedjafari E, et al. Enhanced reconstruction of rat calvarial defects achieved by plasma-treated electrospun scaffolds and induced pluripotent stem cells. *Cell Tissue Res* 2013; 354(3): 849–860.
38. Huang GT, Gronthos S and Shi S. Mesenchymal stem cells derived from dental tissues vs. those from other sources: their biology and role in regenerative medicine. *J Dent Res* 2009; 88(9): 792–806.
39. D'Souza RN, Cavender A, Dickinson D, et al. TGF-beta1 is essential for the homeostasis of the dentin-pulp complex. *Eur J Oral Sci* 1998; 106 Suppl 1: 185–191.
40. Chiang YC, Chang HH, Wong CC, et al. Nanocrystalline calcium sulfate/hydroxyapatite biphasic compound as a TGF- $\beta$ 1/VEGF reservoir for vital pulp therapy. *Dent Mater* 2016; 32(10): 1197–1208.
41. Kim TH, Bae CH, Lee JY, et al. Temporo-spatial requirement of Smad4 in dentin formation. *Biochem Biophys Res Commun* 2015; 459(4): 706–712.
42. Gullard A, Cronney CM, Wu X, et al. Reduced dentin matrix protein expression in Camurati-Engelmann disease transgenic mouse model. *J Cell Physiol* 2016; 231(5): 1106–1113.
43. Yamashiro T, Tummers M and Thesleff I. Expression of bone morphogenetic proteins and Msx genes during root formation. *J Dent Res* 2003; 82(3): 172–176.
44. Elzoghby AO, Samy WM and Elgindy NA. Albumin-based nanoparticles as potential controlled release drug delivery systems. *J Control Release* 2012; 157(2): 168–182.
45. Yang Z, Zhang N, Ma T, et al. Engineered bovine serum albumin-based nanoparticles with pH-sensitivity for doxorubicin delivery and controlled release. *Drug Deliv* 2020; 27(1): 1156–1164.
46. Zhang S, Doschak MR and Uludağ H. Pharmacokinetics and bone formation by BMP-2 entrapped in polyethyleneimine-coated albumin nanoparticles. *Biomaterials* 2009; 30(28): 5143–5155.
47. Jin LJ, Lamster IB, Greenspan JS, et al. Global burden of oral diseases: emerging concepts, management and interplay with systemic health. *Oral Dis* 2016; 22(7): 609–619.

48. Yu C and Abbott PV. An overview of the dental pulp: its functions and responses to injury. *Aust Dent J* 2007; 52: S4–16.
49. Hilton TJ, Ferracane JL and Mancl L; Northwest Practice-based Research Collaborative in Evidence-based Dentistry (NWP). Comparison of CaOH with MTA for direct pulp capping: a PBRN randomized clinical trial. *J Dent Res* 2013; 92(7 Suppl): 16S–22S.
50. Nowicka A, Lipski M, Parafiniuk M, et al. Response of human dental pulp capped with biodentine and mineral trioxide aggregate. *J Endod* 2013; 39(6): 743–747.
51. Sloan AJ and Smith AJ. Stem cells and the dental pulp: potential roles in dentine regeneration and repair. *Oral Dis* 2007; 13(2): 151–157.
52. Arany PR and Mooney DJ. At the edge of translation – materials to program cells for directed differentiation. *Oral Dis* 2010; 17(3): 241–251.
53. Wang R, Bao B, Bao C, et al. Resveratrol and celastrol loaded collagen dental implants regulate periodontal ligament fibroblast growth and osteoclastogenesis of bone marrow macrophages. *Chem Biodivers* 2020; 17(9): e2000295.
54. Rahman SU, Nagrath M, Ponnusamy S, et al. Nanoscale and macroscale scaffolds with controlled-release polymeric systems for dental craniomaxillofacial tissue engineering. *Materials* 2018; 11(8): 1478.
55. Oliva N and Almquist BD. Spatiotemporal delivery of bioactive molecules for wound healing using stimuli-responsive biomaterials. *Adv Drug Deliv Rev* 2020; 161–162: 22–41.
56. Biondi M, Ungaro F, Quaglia F, et al. Controlled drug delivery in tissue engineering. *Adv Drug Deliv Rev* 2008; 60(2): 229–242.
57. Tzavlaki K and Moustakas A. TGF- $\beta$  signaling. *Biomolecules* 2020; 10(3): 487.
58. Bertoneclj V, Pelipenko J, Kristl J, et al. Development and bioevaluation of nanofibers with blood-derived growth factors for dermal wound healing. *Eur J Pharm Biopharm* 2014; 88(1): 64–74.
59. Chen L, Huang Y, Yang R, et al. Preparation of controlled degradation of insulin-like growth factor 1/spider silk protein nanofibrous membrane and its effect on endothelial progenitor cell viability. *Bioengineered* 2021; 12(1): 8031–8042.
60. Cheng G, Ma X, Li J, et al. Incorporating platelet-rich plasma into coaxial electrospun nanofibers for bone tissue engineering. *Int J Pharm* 2018; 547(1–2): 656–666.